J|A|C|S ARTICLES

Published on Web 11/09/2009

Infrared Spectroscopy of Ionophore-Model Systems: Hydrated Alkali Metal Ion 18-Crown-6 Ether Complexes

Jason D. Rodriguez, Timothy D. Vaden, and James M. Lisy*

Department of Chemistry, University of Illinois at Urbana−Champaign, Urbana Illinois 61801

Received July 23, 2009; E-mail: j-lisy@uiuc.edu

Abstract: We report our efforts to study host−guest complexes in the gas phase using a combination of cluster spectroscopy and density functional theory. Mass-selected M^+(18-crown-6 ether)$(H_2O)_{1-4}$ complexes for the alkali metal ion series were probed using infrared predissociation (IRPD) spectroscopy in the OH stretching region. As the degree of hydration is increased, the IRPD spectra undergo significant changes as the strong 18c6···M^+ interaction weakens and allows H_2O···H_2O hydrogen-bonding interactions to compete. The size of the ion is important in determining when this transition occurs. For the smaller ions, Li^+ and Na^+, the 18c6···M^+ interaction proves to be more resilient and is still dominant with two and three waters present. The potassium cation, with its optimum size match with the 18-cown-6 ether cavity, serves as a bridge between the larger and smaller alkali metal ions. In particular, we found a structure for K^+(18-crown-6 ether)$(H_2O)_2$ that appears to be a building block for K^+(18-crown-6 ether)$(H_2O)_3$ complexes and is also believed to be present in Rb^+(18-crown-6 ether)$(H_2O)_{2,3}$ and Cs^+(18-crown-6 ether)$(H_2O)_{2,3}$. With four waters present, we were unable to spectrally resolve features associated with individual water molecules due to broad hydrogen bonding. However, results for Cs^+(18-crown-6 ether)$(H_2O)_4$ suggest that H_2O···H_2O hydrogen bonding has become the dominant interaction present at this size.

1. Introduction

Ionophores play a crucial role in the transport of ions through membranes in biological systems.[1] Despite their importance in many physiological processes, the exact origin for their selective behavior is not well understood. Crown ethers, a prototype for these systems, are an important class of compounds known to preferentially bind certain alkali metal ions in solution. This versatility has led to the use of crown ethers in practical applications such as drug delivery,[2] environmental restoration,[3] and more recently in nanotechnology.[4]

The discovery of the crown ether family by Pederson[5,6] in the 1960s ushered in the era of macrocyclic chemistry.[7] Early condensed-phase work, including many studies by Izatt and co-workers,[8−12] established that the 18-crown-6 ether (18c6) exhibited selectivity for K^+ in aqueous solution.[13] Although a universal explanation has been elusive for describing this behavior, the "best-fit" model[8] has often been used to explain the condensed phase observations. Over the last two decades two new avenues of inquiry, quantum chemical calculations and gas phase techniques, have been used to study crown ether systems. Improvements in the speed and efficiency of CPUs used in quantum chemistry have progressed significantly to allow "large" systems such as crown ethers to be studied using molecular mechanics,[14,15] molecular dynamics,[16,17] Monte Carlo,[18] free energy perturbation techniques,[19] and *ab initio* methods.[20−22] A study by Glendening et al.[20] reported that in the unsolvated M^+(18c6) complex, the binding energy between the crown ether and the smallest alkali metal ion, Li^+, was the greatest. This seemed to contradict the "best-fit" model which favored K^+ being the ideal guest of 18c6 in the condensed phase. Only when a few waters were added to the M^+(18c6) complexes

(1) Gokel, G. W.; Daschbach, M. M. *Coord. Chem. Rev.* **2008**, *252*, 886.
(2) Ju, X.-J.; Liu, L.; Xie, R.; Niu, C. H.; Chu, L.-Y. *Polymer* **2009**, *50*, 922.
(3) Horwitz, E. P.; Dietz, M. L.; Fisher, D. E. *Solvent Extr. Ion Exch.* **1991**, *9*, 1.
(4) Liu, C.; Walter, D.; Neuhauser, D.; Baer, R. *J. Am. Chem. Soc.* **2003**, *125*, 13936.
(5) Pedersen, C. J. *J. Am. Chem. Soc.* **1967**, *89*, 2495.
(6) Pedersen, C. J. *J. Am. Chem. Soc.* **1967**, *89*, 7017.
(7) Izatt, R. M. *Chem. Soc. Rev.* **2007**, *36*, 143.
(8) Izatt, R. M.; Rytting, J. H.; Nelson, D. P.; Haymore, B. L.; Christensen, J. J. *Science* **1969**, *164*, 443.
(9) Izatt, R. M.; Nelson, D. P.; Rytting, J. H.; Haymore, B. L.; Christensen, J. J. *J. Am. Chem. Soc.* **1971**, *93*, 1619.
(10) Izatt, R. M.; Terry, R. E.; Nelson, D. P.; Chan, Y.; Eatough, D. J.; Bradshaw, J. S.; Hansen, L. D.; Christensen, J. J. *J. Am. Chem. Soc.* **1976**, *98*, 7626.
(11) Izatt, R. M.; Terry, R. E.; Haymore, B. L.; Hansen, L. D.; Dalley, N. K.; Avondet, A. G.; Christensen, J. J. *J. Am. Chem. Soc.* **1976**, *98*, 7620.
(12) Lamb, J. D.; Izatt, R. M.; Swain, C. S.; Christensen, J. J. *J. Am. Chem. Soc.* **1980**, *102*, 475.
(13) Pedersen, C. J.; Frensdorff, H. K. *Angew. Chem., Int. Ed.* **1972**, *11*, 16.
(14) Wipff, G.; Weiner, P.; Kollman, P. *J. Am. Chem. Soc.* **1982**, *104*, 3249.
(15) Hay, B. P.; Rustad, J. R.; Hostetler, C. J. *J. Am. Chem. Soc.* **1993**, *115*, 11158.
(16) Dang, L. X. *J. Am. Chem. Soc.* **1995**, *117*, 6954.
(17) Vayssiere, P.; Chaumont, A.; Wipff, G. *Phys. Chem. Chem. Phys.* **2005**, *7*, 124.
(18) Kim, H. S. *J. Phys. Chem. B* **2004**, *108*, 11753.
(19) Wang, J.; Kollman, P. A. *J. Am. Chem. Soc.* **1998**, *120*, 11106.
(20) Glendening, E. D.; Feller, D.; Thompson, M. A. *J. Am. Chem. Soc.* **1994**, *116*, 10657.
(21) Feller, D. *J. Phys. Chem. A* **1997**, *101*, 2723.
(22) Ali, S. M.; Maity, D. K.; De, S.; Shenoi, M. R. K. *Desalination* **2008**, *232*, 181.

did the condensed-phase behavior emerge as K^+ become the preferred guest of the 18c6 macrocycle.[21]

Early gas phase work on the M^+(18c6) systems focused mainly with probing these complexes with mass spectrometric techniques.[23−27] Like the aforementioned theoretical work, there seemed to be an inconsistency between the aqueous and the gas phase trends.[27] Using unsolvated M^+(18c6) complexes generated via liquid secondary ion mass spectrometry, Brodbelt and co-workers found that the "maximum contact point"[24] model was appropriate for gas phase crown ether complexes. In the study, Na^+ was found to be the preferred guest of the 18c6 macrocycle over K^+. This was due primarily to the fact that the smaller Na^+ could maximize the favorable interactions inside the ether cavity.[24] A study by Armentrout and co-workers[28] using guided ion beam techniques to determine bond dissociation energies of Na^+, K^+, Rb^+, and Cs^+ with 18c6 found that smallest alkali metal ion in the series studied, Na^+, was preferentially bound to 18c6 in the gas phase. However, when microsolvation was factored in,[29] like in the theoretical study by Feller,[21] the aqueous phase behavior began to emerge when the M^+(18c6) complexes were solvated with 4−6 waters. This experimental study established that aqueous phase selectivity is not merely influenced by the metal ion−crown ether interaction, but rather a balance of all of the noncovalent interactions present in the systems.[29]

In this study, we report our efforts to identify and characterize the various noncovalent interactions present in M^+(18c6)-$(H_2O)_{1-4}$ complexes (M = Li, Na, K, Rb, and Cs), using infrared predissociation (IRPD) spectroscopy in the OH stretching region of H_2O. The OH stretching region is ideal for studying these systems since the O−H stretch is sensitive to the bonding environment and has been shown to be useful in distinguishing between ion−solvent and hydrogen-bonding interactions.[30] Using mass spectrometric techniques we can track the changes in the IR spectra as a function of stepwise hydration. The combination of these two methods allows us to probe the evolution of noncovalent interactions as the solvation environment changes at the molecular level.

2. Experimental Section

Our experimental apparatus has been described in detail elsewhere,[30] so only a brief overview is presented here. Argon carrier gas seeded with H_2O (~0.1%) is passed through a heated sample holder (90−100 °C) containing crystalline 18c6. The resulting 18c6/H_2O/Ar gas mixture is forced through a 180 μm conical nozzle at a backing pressure of ~450−500 Torr and into the source vacuum chamber. The gas mixture is allowed to fully expand before colliding with alkali metal ions ejected via thermionic emission from a tungsten filament. Nascent cluster ions stabilize via evaporation of H_2O and enter a differentially pumped intermediate chamber via a 2.0 mm skimmer. Cluster ions exiting the skimmer are collected and transported via an octapole ion guide and a stack of electrostatic aperture lenses to the detector chamber, which contains a triple quadrupole mass spectrometer. In the first quadrupole, the parent cluster ions of interest are mass selected. In the second (rf-only) quadrupole, the cluster ions interact with the output of a tunable IR laser (Laser Vision OPO/OPA pumped by a 10 Hz Nd:YAG laser). Fragment ions are observed when the photon energy plus the nascent internal energy of the cluster ion exceeded the binding energy of the most labile ligand. These fragment ions are mass-analyzed by the third quadrupole and the action spectrum is recorded as a function of laser frequency. A three-point averaging procedure was applied to smooth the experimental spectra.

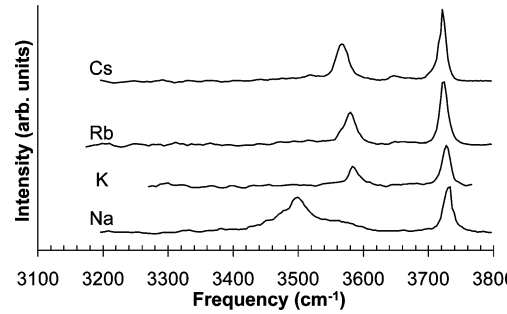

Figure 1. Experimental IRPD spectral summary of $M^+(18c6)(H_2O)_1$ complexes in the OH stretching region.

3. Computational Methods

We performed quantum chemical calculations on the $M^+(18c6)(H_2O)_n$ complexes to assist in the interpretation of our experimental results. Starting geometries of candidate structures were constructed using the Spartan 02 software package.[31] Geometry optimizations and harmonic vibrational frequency calculations were then carried out using density functional theory (DFT) at the B3LYP/6-31+G* level in Gaussian 03.[32] For the larger alkali metal ions (K^+, Rb^+, and Cs^+) the LANL2DZ effective core potential[33−35] was used. Graphical representations of these structures were generated using Molden[36] and are based on the fully optimized geometry calculations using the tight convergence limit. Simulated IR spectra were generated using SWizard.[37] Gaussian line shapes (fwhm 15 cm^{-1}) were used to model the experimental features in the simulated spectra. Calculated frequencies were scaled by a factor of 0.9759 to facilitate comparison with experiments. Free energies were calculated using the THERMO.PL script[38] using the output of the vibrational frequency calculations. Binding energies reported in this work were calculated using the supermolecule method.[39]

4. Results and Discussion

4.1. $M^+(18c6)(H_2O)_1$. The experimental IRPD spectra for $M^+(18c6)(H_2O)_1$ are shown in Figure 1 for M = Na, K, Rb, and Cs. The binding energy of H_2O in the Li^+ $n = 1$ complex is calculated to be 104 kJ/mol. This exceeds the combined energy of a photon and the internal energy of the cluster, so no spectrum was measured for $Li^+(18c6)(H_2O)_1$. All of the IR spectra contain a free OH feature and a prominent hydrogen-

(23) Zhang, H.; Chu, I. H.; Leming, S.; Dearden, D. V. *J. Am. Chem. Soc.* **1991**, *113*, 7415.
(24) Maleknia, S.; Brodbelt, J. *J. Am. Chem. Soc.* **1992**, *114*, 4295.
(25) Dearden, D. V.; Zhang, H.; Chu, I. H.; Wong, P.; Chen, Q. *Pure Appl. Chem.* **1993**, *65*, 423.
(26) Brodbelt, J. S.; Liou, C.-C. *Pure Appl. Chem.* **1993**, *65*, 409.
(27) Abdoul-Carime, H. *J. Chem. Soc., Faraday Trans.* **1998**, *94*, 2407.
(28) More, M. B.; Ray, D.; Armentrout, P. B. *J. Am. Chem. Soc.* **1999**, *121*, 417.
(29) Armentrout, P. B. *Int. J. Mass Spectrom.* **1999**, *193*, 227.
(30) Lisy, J. M. *Int. Rev. Phys. Chem.* **1997**, *16*, 267.
(31) Deppmeier, B. J.; et al. *SPARTAN 2002*, SPARTAN 2002 SGI IRIX 64 (mips4); Irvine, CA, 2002.
(32) Frisch, M. J.; et al. *Gaussian 03*, B.04 ed.; Gaussian: Pittsburgh, PA, 2003.
(33) Hay, P. J.; Wadt, W. R. *J. Chem. Phys.* **1985**, *82*, 270.
(34) Wadt, W. R.; Hay, P. J. *J. Chem. Phys.* **1985**, *82*, 284.
(35) Hay, P. J.; Wadt, W. R. *J. Chem. Phys.* **1985**, *82*, 299.
(36) Schaftenaar, G.; Noordik, J. H. *J. Comput.-Aided Mol. Des.* **2000**, 123.
(37) Gorelsky, S. I. *SWizard program*; http://www.sg-chem.net/ CCRI, University Of Ottawa: Ottawa, Canada, 2008.
(38) Irikura, K. K. Perl Script for Thermochemistry. *THERMO.PL*; National Institute of Standards and Technology: Washington, DC, 2002.
(39) Sapse, A. M.; Russell, C. S. *Int. J. Quantum Chem.* **1984**, *26*, 91.

bonded feature below 3600 cm^{-1}. While there are slight changes in both features with decreasing ion size, the hydrogen-bonded feature for Na^+ is much broader and shifted ~85 cm^{-1} to lower frequency. For K^+, Rb^+, and Cs^+ there is a trend to lower frequency with increasing ion size for the hydrogen-bonded feature at ~3580 cm^{-1}. This seems to indicate that while the binding environment of the H_2O remains constant, there are slight changes with the size of the metal ion. The free OH feature also undergoes a more modest shift to lower frequency with increasing ion size. There also appears to be no indication of the bidentate hydrogen-bonded high energy conformer reported previously[40] for $K^+(18c6)(H_2O)_1Ar_{1-4}$. Since this type of cluster forms via evaporation of Ar, it contains insufficient internal energy to undergo rearrangement to lower-energy conformers following ion impact. In this study, the complexes form primarily via evaporation of H_2O and contain sufficient internal energy to overcome the barriers which lead to lower-energy conformers. For Cs^+ there is also a hint in the experimental spectrum of an OH symmetric stretch located at 3644 cm^{-1}, suggesting the presence of an additional, albeit minor, conformer.

The calculated structures for the $M^+(18c6)(H_2O)_{1-4}$ complexes are shown in Figure 2. The relative Gibbs free energies (ΔG) are also given at 0K/100K/298 K for each alkali metal ion. Calculated structures are arranged according to their relative free energies at 298 K, since complexes formed via evaporation of H_2O in our apparatus have internal energies corresponding to effective temperatures of ~300 K. A more detailed quantitative discussion of evaporative cooling and effective temperatures of species formed in our experiments may be found elsewhere.[41,42] Although the IRPD spectrum for the $Li^+(18c6)(H_2O)_1$ complex could not be acquired due to strong binding of H_2O, we report and discuss the DFT structure. The H_2O is bound directly to 18c6 via a bidentate hydrogen bond, a configuration noted in our previous study[40] of the $K^+(18c6)(H_2O)_1Ar$ complex,. The key difference between these two ions is that the structure of 18c6 is not highly distorted with Li^+ because the cavity is large enough to accommodate both the H_2O and Li^+.

The only conformer found for Na^+ predicts that the ion will sit inside the cavity asymmetrically, closest to three neighboring oxygens to maximize the favorable ion-etheric oxygen interactions. Due to this asymmetric positioning, the H_2O is able to coordinate directly to Na^+ and form a stronger hydrogen bond with an oxygen on the ether in comparison to the larger alkali ions (vide infra). The larger breadth in the hydrogen-bonded feature in the Na^+ case is likely due to somewhat higher internal energy, again due to the stronger binding interactions in this species, compared to that of the larger ions.

The structure for the K^+ case has been reported in our previous study[40] where it was designated to be the traditional (or T) conformer. The IR spectral signature of the warm complex reported here is very similar to the cold argon-tagged T conformer with only a slight shift in the hydrogen-bonded feature of ~5 cm^{-1} to higher frequency for the warm complex compared to the Ar-containing complex. The size match of K^+ (diameter: 2.66 Å) with the size of the 18c6 cavity[43] (diameter: 2.6−3.2 Å) allows the ion to nestle inside the macrocyclic cavity. In contrast to the Na^+ $n = 1$ system, K^+ is symmetrically positioned in the macrocyclic cavity with nearly identical K^+−O

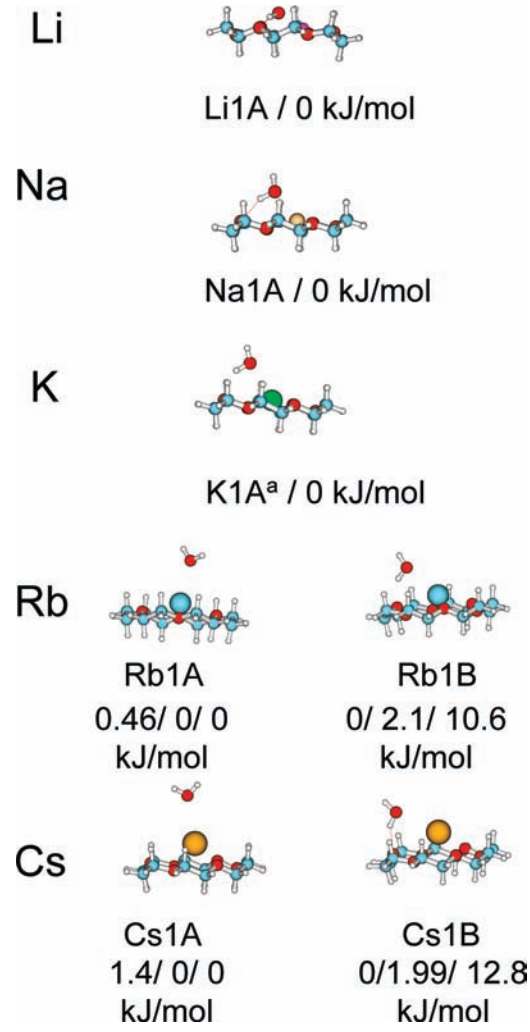

Figure 2. Fully optimized geometries of candidate $M^+(18c6)(H_2O)_1$ conformers at the B3LYP/6-31+G* level of theory. The relative Gibbs free energies (ΔG in kJ/mol) are also given at 0 K/100 K/298 K. The conformers are ordered according to their 298 K energies. [a]The $K^+(18c6)(H_2O)_1$ conformer was previously reported.[40]

distances (~2.824−2.875 Å). The lone H_2O is coordinated to K^+ but is also able to form a hydrogen bond with an etheric 18c6 oxygen. The K^+−O distance for the oxygen participating in the hydrogen bond with H_2O is slightly greater (2.994 Å) compared to the other K^+−O distances. The O···H−O bond angle is 140.43° for K^+ compared with 155.89° for Na^+. This is indicative of a stronger hydrogen bond in the Na^+ case compared to K^+ and is likely why the hydrogen-bonded feature is shifted to lower frequency in the $Na^+(18c6)(H_2O)_1$ experimental spectrum.

For the larger ions, Rb^+ and Cs^+, the mismatch between the 18c6 cavity and the size of the ion plays a crucial role in determining which interactions dominate. The calculated structures, shown in Figure 2, have these two ions sitting above the 18c6 cavity. This is because these ions are too large to fit inside the cavity, without distorting the ether. This changes the interplay between the 18c6···M^+ and 18c6···H_2O interactions slightly, and would seem to make the M^+···H_2O interaction more influential for the larger ions. This is shown in the predicted structures for Rb^+ and Cs^+, as the non-hydrogen-bonded conformers are predicted to be favored over the hydrogen-bonded conformers. In the case of Rb^+, the non-hydrogen-bonded conformer is favored by 10.6 kJ/mol at 298

(40) Rodriguez, J. D.; Lisy, J. M. *Int. J. Mass Spectrom.* **2009**, *283*, 135.
(41) Vaden, T. D.; Weinheimer, C. J.; Lisy, J. M. *J. Chem. Phys.* **2004**, *121*, 3102.
(42) Miller, D. J.; Lisy, J. M. *J. Am. Chem. Soc.* **2008**, *130*, 15393.
(43) Frensdorff, H. K. *J. Am. Chem. Soc.* **1971**, *93*, 600.

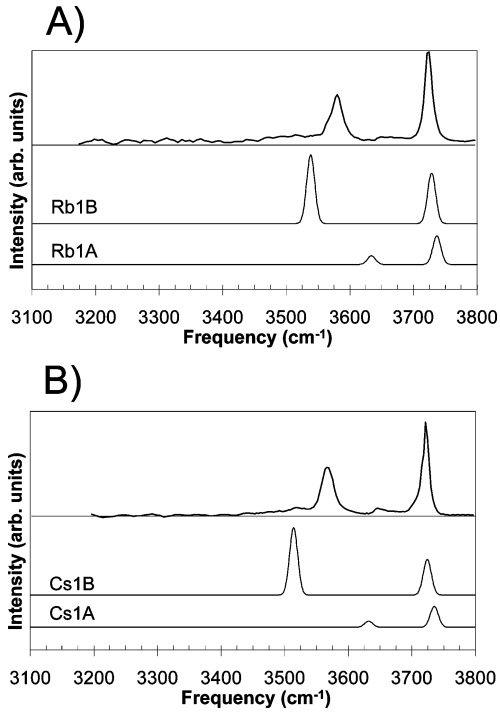

Figure 3. Comparison of experiment and calculations for (A) $Rb^+(18c6)(H_2O)_1$ and (B) $Cs^+(18c6)(H_2O)_1$. The IRPD spectra are shown along with the simulated IR spectra (B3LYP/6-31+G*) for each case.

K. The experimental spectrum for Rb^+ is shown in Figure 3A along with the two lowest-energy conformers. While there is an area of weak intensity ~3640 cm^{-1} where a symmetric stretch may be present, the hydrogen-bonded conformer (Rb1B) is the dominant conformer present in our experiment for Rb^+ based on relative intensities in the IRPD spectrum.

The energy difference between the non-hydrogen-bonded and hydrogen-bonded conformer is 12.8 kJ/mol at 298 K for Cs^+. Figure 3B shows the IRPD spectrum for $Cs^+(18c6)(H_2O)_1$ along with the simulated IR spectra for the predicted conformers. The hydrogen-bonded conformer (Cs1B), like in the case for Rb^+, is clearly the dominant species present in our experiment. For Cs^+, there is however, a noticeable spectral feature in the experimental spectrum at 3640 cm^{-1} that corresponds to the symmetric stretch of the free H_2O in the non-hydrogen-bonded conformer. This mode is shifted ~20 cm^{-1} to lower frequency compared to neutral gas-phase H_2O.[44]

Despite the hint of a symmetric stretch being present in the IRPD spectrum for Cs^+, there is a discrepancy between the experimental results and DFT calculations as to whether the hydrogen-bonded or non-hydrogen-bonded conformers are most stable for $Rb^+(18c6)(H_2O)_1$ and $Cs^+(18c6)(H_2O)_1$. One possibility is that the ensemble of clusters for $Rb^+(18c6)(H_2O)_1$ and $Cs^+(18c6)(H_2O)_1$ in our experiment is colder than our estimated temperature of 298 K. If the temperature of the systems is lower than our estimate, based on the trend of free energies at the various temperatures in Figure 2, the energy spacing between the non-hydrogen-bonded and hydrogen-bonded conformers would decrease and make the Rb1B and Cs1B more favorable in terms of free energy. The trends observed in the free energies in Figure 2 are consistent with previous studies on other "warm" species where conformers with fewer hydrogen bonds are favored over those containing a larger

(44) Fraley, P. E.; Narahari Rao, K. *J. Mol. Spectrosc.* **1969**, *29*, 348.

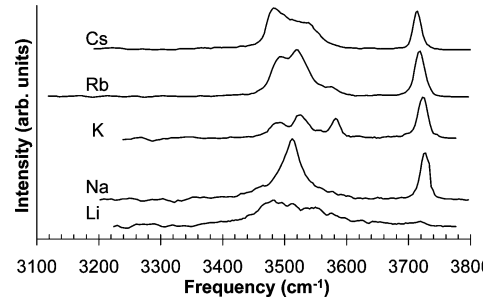

Figure 4. Experimental IRPD spectral summary of $M^+(18c6)(H_2O)_2$ complexes in the OH stretching region.

hydrogen-bonded networks due to entropic considerations.[42] Another possibility, which will be discussed further in the $M^+(18c6)(H_2O)_3$ complexes section (*vide infra*), is that the experiments preferentially sample conformers formed from larger hydrated species that more readily undergo evaporation of H_2O than their more stable counterparts.

4.2. $M^+(18c6)(H_2O)_2$. The IRPD spectra for the $M^+(18c6)(H_2O)_2$ complexes are shown in Figure 4. For Li^+, the IRPD spectrum is broad and featureless containing only a single feature centered ~3500 cm^{-1}. The $n = 2$ experimental spectrum for Na^+ is strikingly similar to the $n = 1$ spectrum (shown in Figure 1), with a single relatively broad feature centered at 3510 cm^{-1}. Compared to $n = 1$ spectra, the biggest changes occur in the systems with the larger ions; there is a significant increase in the hydrogen-bonded OH region due primarily to $H_2O\cdots H_2O$ interactions, now possible with two waters present. The $K^+(18c6)(H_2O)_2$ spectrum has three distinct hydrogen-bonded features at 3480, 3520, and 3579 cm^{-1}. For the two largest ions in the series, there exist broad doublet features at ~3480 and 3520 cm^{-1} for Rb^+ and ~3480 and 3541 cm^{-1} for Cs^+. As in the $n = 1$ systems, the spectra (starting with Na^+) exhibit a free OH feature that shifts slightly, to lower frequency, as the ion size increases.

The fully optimized geometries based on the DFT calculations are shown in Figure 5. Since the Li^+ $n = 2$ spectrum is broad and featureless, it is impossible to assign particular features to the experimental spectrum. However, we have found two low-lying energy isomers for $Li^+(18c6)(H_2O)_2$. The sandwich-type conformer (Li2A) is found to be slightly more energetically favored over the same side-type conformer (Li2B). The latter conformer seems to continue to build on the $n = 1$ predicted structure with the first H_2O binding via a bidentate hydrogen bond to 18c6. The second H_2O is coordinated rather rigidly to the Li^+ and is not able to interact with the bidentate H_2O. The Li2A conformer features both waters bound to the system in a configuration where the free OH oscillators of both waters are parallel to the 18c6 plane. This is in sharp contrast to the sandwich-type H_2O configurations of the other alkali ions in Figure 5, where the free OH group is usually nearly perpendicular to the 18c6 plane. If the Li2A isomer is indeed dominant, this may explain the lack of intensity in the free OH stretching region for $Li^+(18c6)(H_2O)_2$.

The IRPD spectrum for $Na^+(18c6)(H_2O)_2$ is shown in Figure 6A along with the simulated IR spectra for its predicted structures. Although the relative energy spacing between the different conformers at 298 K is only 7.6 kJ/mol, the Na2B conformer seems to be ruled out based on comparisons with the experiment. The two remaining conformers have similar IR signatures, although their relative intensities are different. Since Na2C replicates the experiment best, we believe it to be the

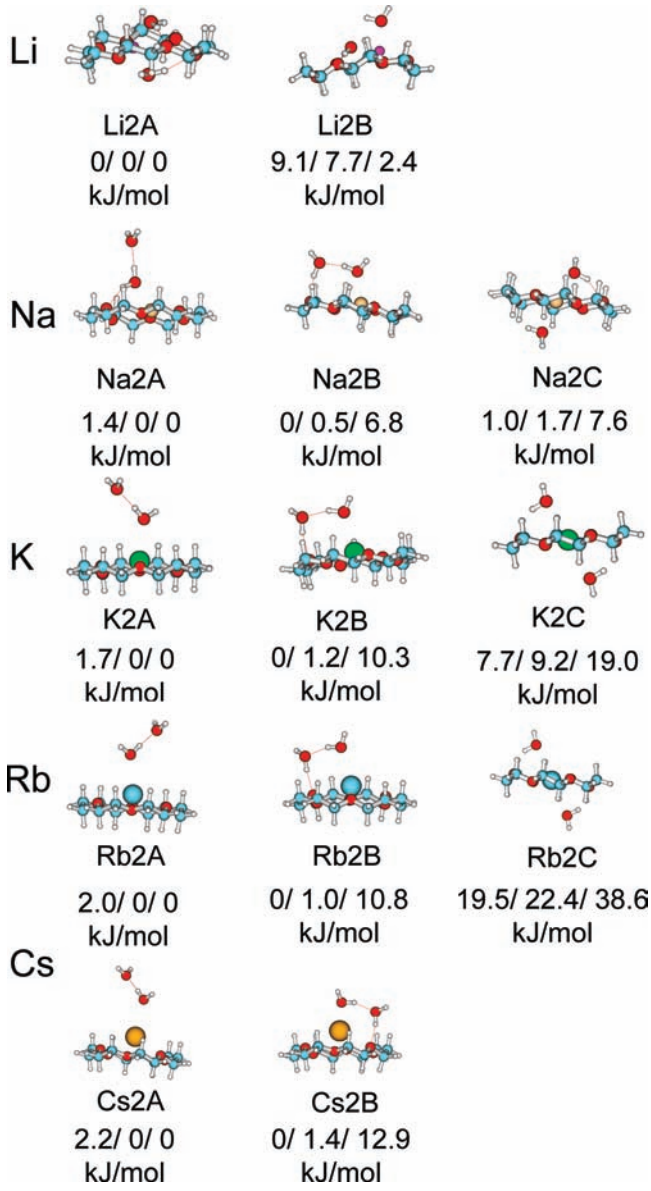

Figure 5. Fully optimized geometries of candidate $M^+(18c6)(H_2O)_2$ conformers at the B3LYP/6-31+G* level of theory. The relative Gibbs free energies (ΔG in kJ/mol) are also given at 0 K/100 K/298 K. The conformers are ordered according to their 298 K energies.

main conformer present (although Na2A may still be present as a minor contributor). This conformer features a sandwich type configuration with one H_2O above and another below the 18c6. However, the waters are not exactly identical since the top H_2O has a slightly longer hydrogen bonded O−H bond distance (0.979 Å) than the bottom H_2O (0.975 Å). The O···H−O bond angle is also slightly greater for the top H_2O (149.30°) compared to the bottom H_2O (131.54°). The existence of Na2C as the major conformer in our experiment shows that for Na^+, the $H_2O\cdots H_2O$ hydrogen bonding interaction is not yet favored over the 18c6···M^+, 18c6···H_2O, and $M^+\cdots H_2O$ interactions. The previous study by Feller[21] also found the n2C-type conformer to be the predicted structure for $Na^+(18c6)(H_2O)_2$.

The IRPD spectrum for the K^+ system is the most intriguing spectrum of the series (shown in Figure 4). It is clearly different from all of the other spectra in that it has three clearly resolved hydrogen-bonded features. The three conformers predicted for

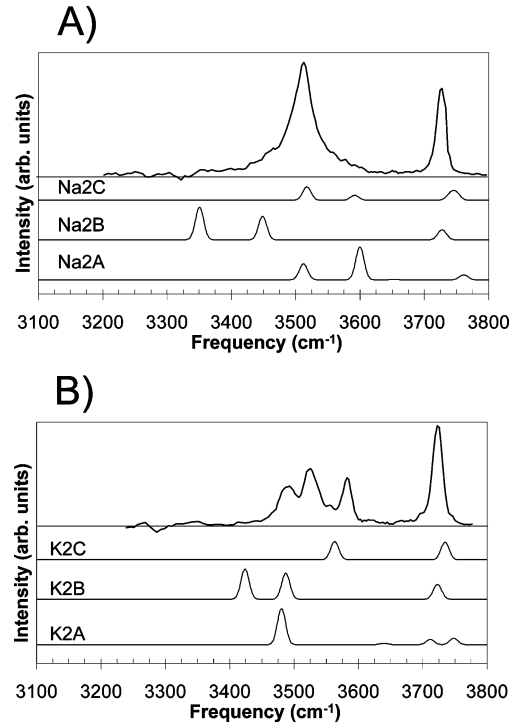

Figure 6. Comparison of experiment and calculations for (A) $Na^+(18c6)(H_2O)_2$ and (B) $K^+(18c6)(H_2O)_2$. The IRPD spectra are shown along with the simulated IR spectra (B3LYP/6-31+G*) for each case.

$K^+(18c6)(H_2O)_2$ (shown in Figure 5) are similar to those found for Na^+. The IRPD spectrum for $K^+(18c6)(H_2O)_2$ is shown in Figure 6B along with the simulated IR spectra for its three predicted structures. Unlike Na^+, the energy spacing for the three K^+ conformers is substantial. Based on the comparison of the calculated spectra in Figure 6B with the experimental spectrum, it appears that all three conformers are present in our experiment. Conformers K2A and K2B seem to replicate the two lowest-frequency hydrogen-bonded features, although they underestimate the experimental frequencies. Both K2A and K2B have a calculated spectral feature at ~3480 cm^{-1} which likely gives rise to the most intense feature in the IRPD spectrum (3525 cm^{-1}). However, the calculations suggest that the origin of this calculated feature is not the same in each case. In K2A the calculated spectral feature at ~3480 cm^{-1} is due to the $H_2O\cdots H_2O$ hydrogen bond, while in K2B it is due to the 18c6···H_2O hydrogen bond. The other hydrogen-bonded OH feature in K2B at ~3415 cm^{-1} is due to the $H_2O\cdots H_2O$ hydrogen-bonding interaction and is likely responsible for the hydrogen-bonded OH band near 3490 cm^{-1} in the experiment. There is only a very minor hint of a symmetric feature (due to the proton-accepting H_2O in K2A) in the experimental spectrum in the ~3640 cm^{-1} region. The simulated IR spectrum, however, predicts this feature to be weak. The highest-frequency hydrogen-bonded feature is not replicated by K2A or K2B, the two lowest-energy conformers. This feature, however, matches well with conformer K2C. Both waters in K2C are identical to the lone hydrogen-bonded water in conformer K1A (shown in Figure 2). Expectedly, both $n = 1$ and 2 experimental spectra for K^+ have a feature due to this type of hydrogen bond at 3580 cm^{-1}. Unlike conformer Na2C, which has inequivalent waters forming the sandwich-type complex, both waters in K2C are identical. While the presence of this high-energy conformer (19 kJ/mol higher in relative energy at 100 K compared to K2A) is unexpected, there is a possible (and plausible) explanation. The

binding energy of the second (bottom) H_2O in K2C is 24.8 kJ/mol. This value is significantly lower than the binding energy of the second H_2O in K2A or K2B which is 30.8 and 32.6 kJ/mol, respectively. This trend indicates that in K2C the 18c6 macrocycle is effective in sequestering K^+. The ion−ionophore binding is optimized to the point where solvation of K^+ by H_2O is less favorable, causing the increased relative energy of conformer K2C. In other words, the attempt by K^+ to coordinate *both* water molecules while interacting with the 18c6 is clearly unfavorable, in comparison to the interactions depicted in structures K2A and K2B. This agrees well with the condensed-phase picture of K^+ being the ideal guest for 18c6, and indicates that in conformer K2C the 18c6···K^+ interaction is clearly the most dominant force present. This is not the case for the Na2C conformer, where strong interactions between both waters, Na^+ and the ether, are possible due to the smaller size of the cation. As the number of waters increases, H_2O···H_2O interactions will be able to weaken this particular configuration, utilizing the size mismatch between the ion and the 18c6 cavity. The existence of all three conformers in our experiment indicates that for K^+, where size of the ion and the 18c6 cavity have the closest match, we see evidence of 18c6···M^+, 18c6···H_2O, M^+···H_2O, and H_2O···H_2O interactions.

Since the IRPD spectra for Rb^+ and Cs^+ have only broad hydrogen bonds, assigning particular conformers to the experiment is not practical. However using the assignments for Na^+ and K^+, the contributions to the IRPD spectra for Rb^+ and Cs^+ can be deconvoluted. The experimental spectrum for Rb^+ contains hydrogen-bonded transitions at ~3480 and 3520 cm^{-1} and a small feature at ~3580 cm^{-1}. These are essentially the same positions for the hydrogen-bonded features already assigned for K^+. The only key difference is that for Rb^+ the relative populations for the conformers in the experiment are different. Based on the IRPD spectra, and using our previous assignments for K^+, it is likely that both of the lowest-energy conformations, Rb2A and Rb2B, are present in the experiment. Since the experimental spectrum for Rb^+ has more intensity in the ~3480 cm^{-1} region, it is possible that conformer Rb2B contributes to the $Rb^+(18c6)(H_2O)_2$ spectrum more significantly than its analogue (K2B) played in $K^+(18c6)(H_2O)_2$. This was the predicted conformer found by Feller[21] for Rb^+. The preference for this type of conformer over the other two is clearly shown in the structure (shown in Figure 5). Conformer Rb2B allows Rb^+ to lie above the 18c6 cavity and avoid the energy increase of lying too close to the 18c6 cavity.[21] The highest-energy conformer is once again predicted to be the sandwich-type conformer (Rb2C). This conformer may have a minor role in our experiment, possibly responsible for the very weak shoulder at ~3580 cm^{-1}.

Only two stable conformers, Cs2A and Cs2B, were found for $Cs^+(18c6)(H_2O)_2$ (shown in Figure 5). As shown in Figure 4, there is a clear increase in the hydrogen-bonded OH stretch intensity at ~3480 cm^{-1} in going from K^+ to Cs^+. These features were previously attributed to the same-side H_2O arrangement with two hydrogen bonds. While we believe both conformers Cs2A and Cs2B to be present in our experiment, it is likely that conformer Cs2B, despite being higher in relative energy, is the major conformer since it features same-side H_2O arrangement with two hydrogen bonds. In conformer Cs2B, Cs^+ is afforded the ability to avoid the energy cost of sitting too close to the 18c6 cavity by the double hydrogen-bonded arrangement of the waters, which serve to "extract" the ion from the 18c6. Expectedly, there is also no indication of the 18c6···H_2O hydrogen bond at ~3580 cm^{-1} due to sandwich-type configuration in the $Cs^+(18c6)(H_2O)_2$ experimental spectrum. This makes sense since Cs^+ is much too large for the 18c6 cavity. The increase in the intensity of H_2O···H_2O hydrogen bonding shown in Figure 4 in going from K^+ to Cs^+ is indicative of a strong correlation between ion size and noncovalent interactions present. As the size of the ion increases, the ion prefers to sit farther above the 18c6 cavity. This trend weakens the 18c6···M^+ and 18c6···H_2O interactions substantially, and allows the M^+···H_2O and H_2O···H_2O interactions to dominate.

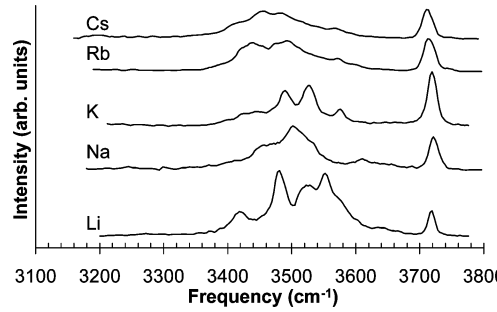

Figure 7. Experimental IRPD spectral summary of $M^+(18c6)(H_2O)_3$ complexes in the OH stretching region.

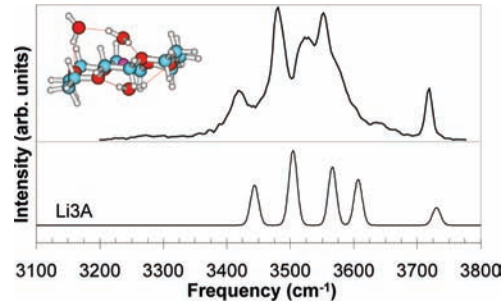

Figure 8. Comparison between experiment and calculations for $Li^+(18c6)(H_2O)_3$. Only one low-lying conformer was found for $Li^+(18c6)(H_2O)_3$ at the B3LYP/6-31+G* level of theory. The agreement between the experimental and simulated spectra indicates conformer Li3A is the major conformer present in the experiment.

4.3. $M^+(18c6)(H_2O)_3$. The IRPD spectra for the $n = 3$ complexes are shown in Figure 7. With three waters present, all of the spectra exhibit a noticeable increase in hydrogen bonding and we are able to observe resolvable features for Li^+ for the first time. With the binding energy of the third water (~37 kJ/mol) for $Li^+(18c6)(H_2O)_3$ comparable to the photon energy, photodissociation is more facile and the experimental spectrum contains four distinct transitions in the hydrogen-bonding region at 3415, 3477, 3522, and 3552 cm^{-1}. For Na^+, $n = 3$ has a broad feature that dominates the IRPD spectrum at ~3500 cm^{-1}, as was the case for $n = 1$ and 2 The experimental spectrum for $K^+(18c6)(H_2O)_3$ contains three resolvable hydrogen-bonded features at 3486, 3525, and 3573 cm^{-1}. Additionally, there is a broader, weaker feature near 3430 cm^{-1}. The experimental spectra for the largest alkali metal ions, Rb^+ and Cs^+, contain broad hydrogen-bonded OH bands that span over 200 cm^{-1} and are centered below 3500 cm^{-1}. All of the cluster ions display free OH bands near 3720 cm^{-1}.

For $Li^+(18c6)(H_2O)_3$, only one low-lying conformer was found (Li3A). Its corresponding simulated IR spectrum is shown in Figure 8 along with the experimental spectrum. This conformer does a remarkable job in replicating the IRPD spectrum. The most fascinating aspect of the Li3A structure is that Li^+ prefers to stay inside the 18c6 cavity. This is possible

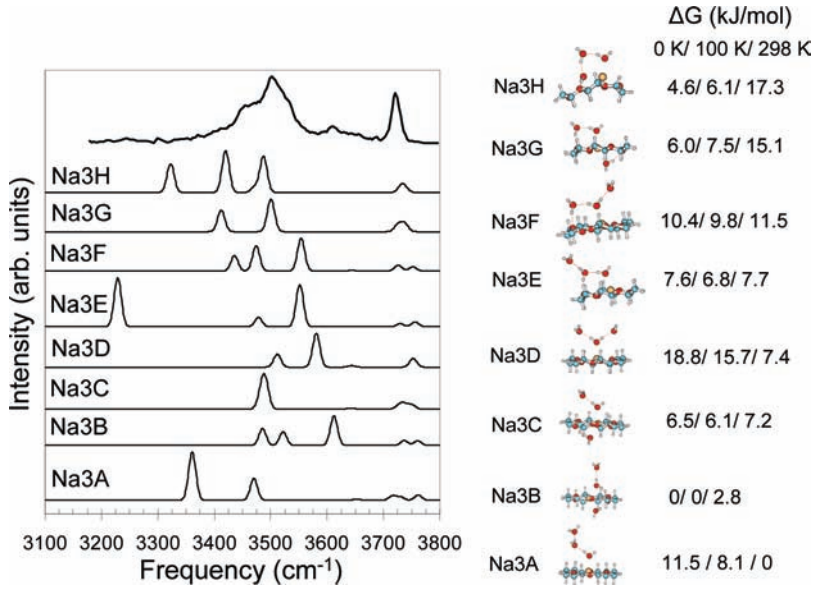

Figure 9. Comparison of experiment and calculations for $Na^+(18c6)(H_2O)_3$. The IRPD spectra are shown along with the simulated IR spectra (B3LYP/6-31+G*) for eight candidate conformers. The relative Gibbs free energies (ΔG in kJ/mol) are also given at 0 K/100 K/298 K. The conformers are ordered according to their 298 K energies.

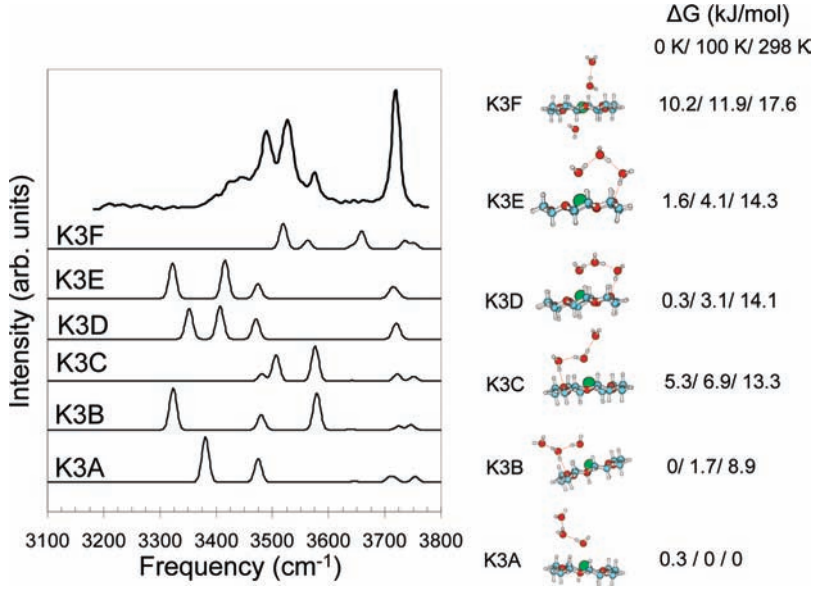

Figure 10. Comparison of experiment and calculations for $K^+(18c6)(H_2O)_3$. The IRPD spectra are shown along with the simulated IR spectra (B3LYP/6-31+G*) for six candidate conformers. The relative Gibbs free energies (ΔG in kJ/mol) are also given at 0 K/100 K/298 K. The conformers are ordered according to their 298 K energies.

due to the size mismatch between the cavity and the Li^+, where water molecules can work into a position between the ion and still strongly intereact with the crown ether (as can be seen by comparing with the structure of Li2A).

The comparison between the experimental spectrum for $Na^+(18c6)(H_2O)_3$ and its calculated conformers is shown in Figure 9. There are five conformers within 7.7 kJ/mol at 298 K for $Na^+(18c6)(H_2O)_3$. Although conformer Na3D seems to model the experiment the best, we cannot assign it as being the only conformer populated in the experiment since Na3B and Na3F also come close in modeling the IRPD spectrum. One feature that seems particularly interesting in the experimental spectrum for $Na^+(18c6)(H_2O)_3$ is the broad feature just above 3600 cm^{-1}. This is the region where the hydrogen bond due to a double-donor H_2O is expected to appear.[45] As can be seen in the optimized geometries in Figure 9, such a H_2O is present in Na3B, Na3D, Na3E, and Na3F. Of these, all except Na3E are expected to contribute to the experimental spectrum. The low-frequency feature in Na3E is clearly not apparent in the experiment.

The comparison between experimental and calculated spectra for $K^+(18c6)(H_2O)_3$ is shown in Figure 10. With the exception of a broad feature at ~3430 cm^{-1} in the experimental spectrum of $K^+(18c6)(H_2O)_3$, the overall spectral profile continues the trends established for $K^+(18c6)(H_2O)_2$. Unlike $Na^+(18c6)(H_2O)_3$,

(45) Shin, J. W.; Hammer, N. I.; Diken, E. G.; Johnson, M. A.; Walters, R. S.; Jaeger, T. D.; Duncan, M. A.; Christie, R. A.; Jordan, K. D. *Science* **2004**, *304*, 1137.

where a group of candidate conformers were spaced by a relatively small energy difference, conformer K3A is clearly the most energetically favored $K^+(18c6)(H_2O)_3$ conformer at 298 K. The next-nearest conformer, K3B, is higher in energy by 8.9 kJ/mol at 298 K. Whereas, sandwich-type conformers were among the low-energy candidate conformers for Na^+ $n = 3$, only K3F features such a configuration. Both of the smaller ions, Li^+ and Na^+, feature waters on either side of the macrocycle. The calculations indicate that this orientation is not favored for $K^+(18c6)(H_2O)_3$. As in the case of K2C, it appears that the 18c6 is binding K^+ so effectively, that further solvation by more than one H_2O is not favored. Subsequent waters prefer to bind to other waters, indicating that the strong 18c6···K^+ interaction is driving the formation of H_2O···H_2O hydrogen bonds and, to a somewhat lesser extent, 18c6···H_2O hydrogen bonds. While it would seem that conformers K3D and K3E come close to replicating the overall spectral profile in the experiment, they are higher in energy by 14.1 and 14.3 kJ/mol, respectively, at 298 K relative to K3A. Since these species are "warm", a likely possibility is that multiple conformers are being populated in the experiment. With the exception of K3F, all of the conformers shown in Figure 10 may be attributed to portions of the experimental spectrum, although no conformer replicates the experiment on its own. The existence of the two lowest-energy conformers in the experiment is particularly important in modeling the broad feature at ~3430 cm^{-1}. Conformers K3A and K3B differ only in the orientation of the second-shell H_2O. In K3A this H_2O is a single-donor H_2O forming a hydrogen bond with the third-shell H_2O. The second H_2O in K3B is a double-donor H_2O, forming a hydrogen bond with both the third-shell H_2O and with 18c6 via the 18c6···H_2O hydrogen bond. The lowest-frequency band in the calculated spectra of K3A and K3B is due to the hydrogen-bonded interaction of the first- and second-shell waters. The formation of the 18c6···H_2O hydrogen bond in K3B increases the basicity of the second-shell (double-donor) H_2O and leads to the formation of a stronger hydrogen bond between the first- and second-shell waters. This is evidenced by a slightly longer hydrogen-bonded O−H bond length for the first water in K3B (0.990 Å) compared to that for K3A (0.987 Å). In the simulated spectrum of K3B, the formation of this stronger hydrogen bond leads to a shift in the lowest-frequency hydrogen-bonded feature of about 57 cm^{-1} compared to that of K3A. In our experiment, both K3A and K3B are likely to be present, and the rapid conversion of the second-shell water's configuration (from a double-donor to a single-donor) is manifested in the broad nature of the ~3430 cm^{-1} feature. The zero-point energy difference between the K3A and K3B is only 0.3 kJ/mol, indicating that interconversion between the two conformers is likely.

The three lowest-energy conformers for $K^+(18c6)(H_2O)_3$ at 298 K also have the K2B-type substructure present which indicates that it is still the preferred binding motif for $n = 3$ and waters prefer to add to the substructure rather than adopting a completely different configuration. In this study, a recurring trend is that species relatively higher in energy [such as the hydrogen-bonded conformers for $Rb^+(18c6)(H_2O)_1$ and Cs^+-$(18c6)(H_2O)_1$ or conformer K2B of $K^+(18c6)(H_2O)_2$] seem to better replicate the experimental results. We can explain these results by considering the energetics (based on zero-point energies) of $K^+(18c6)(H_2O)_3$ conformer, K3A, as it rearranges to form one of the three $K^+(18c6)(H_2O)_2$ complexes in Figure 11. The greater the binding energy of H_2O in the complex, the less readily it will evaporate a H_2O. Since the complexes

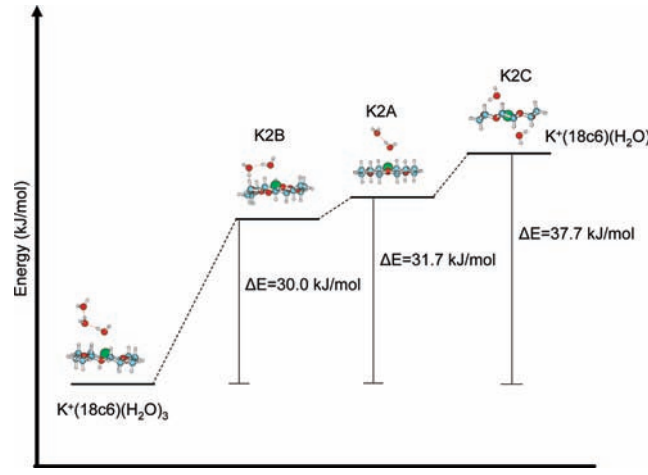

Figure 11. Rearrangement of the $K^+(18c6)(H_2O)_3$ conformer K3A following evaporation of H_2O. The most energetically favored species formed is the K2B $n = 2$ complex. The energies reported are the zero-point relative binding energies calculated using the supermolecule method (ref 39) and are based on the harmonic vibrational frequency calculations done at the B3LYP/6-31+G* level of theory.

generated in this study stabilize solely via evaporation of H_2O, the conformers preferentially populated in the $K^+(18c6)(H_2O)_2$ experiments form from $K^+(18c6)(H_2O)_3$ complexes with the lowest H_2O binding energies. As shown in Figure 11, upon evaporation, the lowest-energy pathway connects conformer K3A to conformer K2B. Thus, in our experiment we would expect to preferentially observe K2B over the other two conformations, K2A and K2C, which is indeed the case. This may be the reason that, despite their higher relative energies, we see the K2B-type conformers for K^+, Rb^+, and Cs^+. The discrepancy noted earlier between the DFT calculations and the IRPD experiments in $Rb^+(18c6)(H_2O)_1$ and $Cs^+(18c6)(H_2O)_1$ may also be influenced by the preferential formation of K2B-type conformers (Rb2B and Cs2B). In the case of the Cs2B conformation of $Cs^+(18c6)(H_2O)_2$, it is more energetically favored by 1.4 kJ/mol to rearrange to the Cs1B conformation over the Cs1A conformer. The higher energy is likely due to the need to break two hydrogen bonds in Cs2B to form Cs1A. This agrees well with Figure 3B, which clearly shows conformer Cs1B as the major conformer present in the experiment.

For $Rb^+(18c6)(H_2O)_3$ and $Cs^+(18c6)(H_2O)_3$ the spectra are broad and lack specific spectral features for a comparison with the results from the DFT calculations. It is noteworthy that these two large ions exhibit extensive H_2O···H_2O hydrogen-bonding interactions in the IRPD spectra.

4.4. $M^+(18c6)(H_2O)_4$. The IRPD spectra for the $n = 4$ complexes are shown in Figure 12. For the entire series, the spectra are dominated by broad hydrogen-bonding features below 3600 cm^{-1}. The breadth of these features indicates that with four waters present, H_2O···H_2O hydrogen bonding is extensive, and this precludes individual assignment of features. Interestingly, only two stable conformers were found for $Cs^+(18c6)(H_2O)_4$ as part of this analysis and are shown in Figure 13. The lowest-energy conformer, Cs4A, contains a cyclic H_2O tetramer configuration, while a second conformer, Cs4B, contains a cyclic H_2O trimer with one of the waters donating a proton to the fourth H_2O. The existence of similar cyclic H_2O configurations in neutral[46−49] and anionic systems[50,51] has been

(46) Pugliano, N.; Saykally, R. J. *Science* **1992**, *257*, 1937.

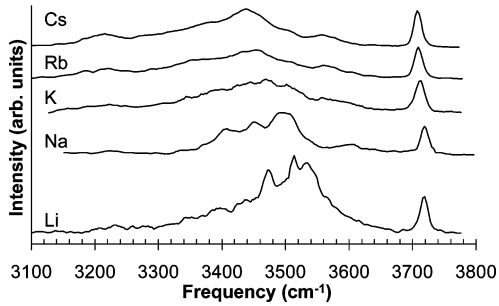

Figure 12. Experimental IRPD spectral summary of $M^+(18c6)(H_2O)_4$ complexes in the OH stretching region.

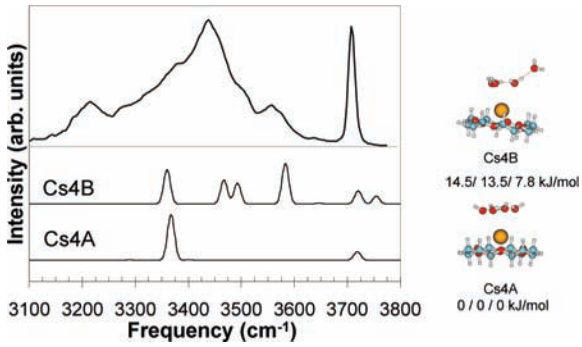

Figure 13. Comparison of experiment with calculations for $Cs^+(18c6)(H_2O)_4$. While both conformers are likely populated in the experiment, the Cs4B conformer reproduces the experimental spectrum better. The relative Gibbs free energies (ΔG in kJ/mol) are also given at 0 K/100 K/298 K. The conformers are ordered according to their 298 K energies.

previously reported. In both $Cs^+(18c6)(H_2O)_4$ conformers there is no evidence of 18c6···H_2O interactions, as Cs^+ acts as an intermediary between the water cluster and 18c6. The experimental and calculation comparison in Figure 13 shows that conformer Cs4B is present as it can produce the feature at ~3580 cm^{-1}. Conformer Cs4B was also predicted to be the minimum-energy conformer in the study by Feller.[21] The feature in the $Cs^+(18c6)(H_2O)_4$ spectrum at ~3200 cm^{-1} is due to the H_2O bend-overtone, "borrowing" intensity from the strong hydrogen-bonded O−H stretching modes at slightly higher frequency.[52]

5. Conclusions

In one of the first comprehensive studies aimed at studying crown ether selectivity using IR spectroscopy, $M^+(18c6)(H_2O)_{1-4}$ complexes (where M = Li, Na, K, Rb, and Cs) were generated in the gas phase. Using IR and mass spectrometric techniques, we have been able to track the IRPD spectra as a function of increasing microhydration. With only one H_2O present, the $M^+(18c6)(H_2O)_1$ complexes have IRPD spectra that are quite similar and show that the 18c6···M^+ interaction is dominant and the 18c6···H_2O and M^+···H_2O interactions have somewhat equal strength. With $n = 2$, H_2O···H_2O interactions now become possible. For the smaller ions, Li^+ and Na^+, the 18c6···M^+ and M^+···H_2O interactions appear to take precedence over the H_2O···H_2O interactions. The size of these ions is small compared to that of the 18c6 cavity. This allows the additional waters to build on the stable 18c6···M^+ moiety. The $K^+(18c6)(H_2O)_2$ system appears to be the most interesting complex in the study. Since the size of the 18c6 cavity matches well with the size of K^+, we are able to identify three different configurations for $K^+(18c6)(H_2O)_2$. These three conformers for $K^+(18c6)(H_2O)_2$ elucidate the delicate balance of the 18c6···M^+, 18c6···H_2O, M^+···H_2O, and H_2O···H_2O interactions present in this system. We see that K^+ is a bridge between the smaller ions (Li^+ and Na^+) and larger ions (Rb^+ and Cs^+). Most importantly we have identified a structural motif, associated with one conformer, K2B, which is particularly significant. It is reflected in the $n = 2$ Rb^+ and Cs^+ structures, and for the K^+ $n = 3$ conformers. The K2B structure features both waters present on the same side, forming 18c6···H_2O and H_2O···H_2O hydrogen bonds. The prominent role of the K2B-type structures in this study is surprising due to its higher-energy compared to lower-energy conformers. This may be due to the evaporation of H_2O from larger clusters to more readily form the K2B-type structure. For the tri- and tetrahydrated systems, the IRPD spectra are dominated by broad H_2O···H_2O hydrogen bonds which preclude detailed comparison with the DFT calculations. For $Cs^+(18c6)(H_2O)_4$ where H_2O···H_2O hydrogen-bonding interactions are believed to be the single most dominant noncovalent interaction present, our DFT calculations predict that one of the preferred configuration features a cyclic H_2O trimer (with the fourth H_2O hydrogen-bonded to one of the trimer waters) interaction with the cesium ion in agreement with previous studies. This important result indicates that with a sufficient hydration sphere, the once dominant 18c6···M^+ interaction can be counterbalanced by H_2O···H_2O and M^+−H_2O interactions.

Acknowledgment. We thank the National Science Foundation (Grants CHE-0415859 and CHE-0748874) for partial support of this research. Acknowledgment is made to the Donors of the American Chemical Society Petroleum Research Fund for partial support of this research. Computational work was done on NCSA Cobalt Supercomputer System (Award No. TG-CHE070097).

Supporting Information Available: Full citations for references 31 and 32. This material is available free of charge via the Internet at http://pubs.acs.org.

JA906185T

(47) Cruzan, J. D.; Braly, L. B.; Liu, K.; Brown, M. G.; Loeser, J. G.; Saykally, R. J. *Science* **1996**, *271*, 59.
(48) Liu, K.; Cruzan, J. D.; Saykally, R. J. *Science* **1996**, *271*, 929.
(49) Burnham, C. J.; Xantheas, S. S.; Miller, M. A.; Applegate, B. E.; Miller, R. E. *J. Chem. Phys.* **2002**, *117*, 1109.
(50) Ayotte, P.; Weddle, G. H.; Johnson, M. A. *J. Chem. Phys.* **1999**, *110*, 7129.
(51) Shin, J.-W.; Hammer, N. I.; Headrick, J. M.; Johnson, M. A. *Chem. Phys. Lett.* **2004**, *399*, 349.
(52) Robertson, W. H.; Weddle, G. H.; Kelley, J. A.; Johnson, M. A. *J. Phys. Chem. A* **2002**, *106*, 1205.